SINTEF
PROCEEDINGS
2

Proceedings of the 12th International Conference on Computational Fluid Dynamics in the Oil & Gas, Metallurgical and Process Industries

Progress in Applied CFD – CFD2017

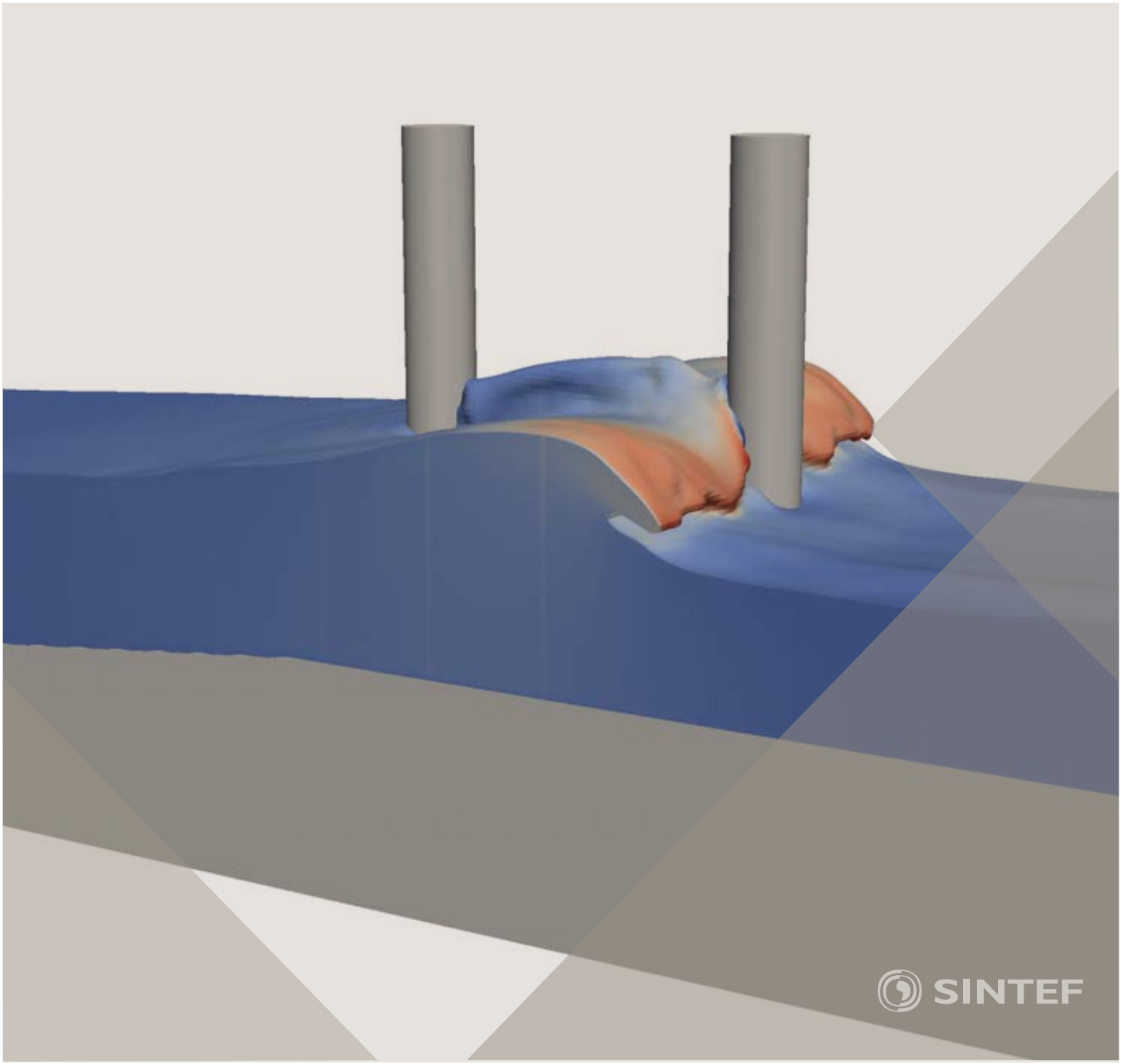

SINTEF Proceedings

Editors:
Jan Erik Olsen and Stein Tore Johansen

Progress in Applied CFD – CFD2017

Proceedings of the 12th International Conference on Computational Fluid Dynamics in the Oil & Gas, Metallurgical and Process Industries

SINTEF Academic Press

SINTEF Proceedings no 2
Editors: Jan Erik Olsen and Stein Tore Johansen
Progress in Applied CFD – CFD2017
Selected papers from 10th International Conference on Computational Fluid Dynamics in the Oil & Gas, Metallurgical and Process Industries

Key words:
CFD, Flow, Modelling

Cover, illustration: Arun Kamath

ISSN 2387-4295 (online)
ISBN 978-82-536-1544-8 (pdf)

SINTEF Academic Press
Address: Forskningsveien 3 B
PO Box 124 Blindern
N-0314 OSLO
Tel: +47 73 59 30 00
Fax: +47 22 96 55 08

www.sintef.no/byggforsk
www.sintefbok.no

SINTEF Proceedings
SINTEF Proceedings is a serial publication for peer-reviewed conference proceedings on a variety of scientific topics.
The processes of peer-reviewing of papers published in SINTEF Proceedings are administered by the conference organizers and proceedings editors. Detailed procedures will vary according to custom and practice in each scientific community.

PREFACE

This book contains all manuscripts approved by the reviewers and the organizing committee of the 12th International Conference on Computational Fluid Dynamics in the Oil & Gas, Metallurgical and Process Industries. The conference was hosted by SINTEF in Trondheim in May/June 2017 and is also known as CFD2017 for short. The conference series was initiated by CSIRO and Phil Schwarz in 1997. So far the conference has been alternating between CSIRO in Melbourne and SINTEF in Trondheim. The conferences focuses on the application of CFD in the oil and gas industries, metal production, mineral processing, power generation, chemicals and other process industries. In addition pragmatic modelling concepts and bio-mechanical applications have become an important part of the conference. The papers in this book demonstrate the current progress in applied CFD.

The conference papers undergo a review process involving two experts. Only papers accepted by the reviewers are included in the proceedings. 108 contributions were presented at the conference together with six keynote presentations. A majority of these contributions are presented by their manuscript in this collection (a few were granted to present without an accompanying manuscript).

The organizing committee would like to thank everyone who has helped with review of manuscripts, all those who helped to promote the conference and all authors who have submitted scientific contributions. We are also grateful for the support from the conference sponsors: ANSYS, SFI Metal Production and NanoSim.

Stein Tore Johansen & Jan Erik Olsen

Organizing committee:

Conference chairman: Prof. Stein Tore Johansen
Conference coordinator: Dr. Jan Erik Olsen
Dr. Bernhard Müller
Dr.Sigrid Karstad Dahl
Dr.Shahriar Amini
Dr.Ernst Meese
Dr.Josip Zoric
Dr.Jannike Solsvik
Dr.Peter Witt

Scientific committee:

Stein Tore Johansen, SINTEF/NTNU
Bernhard Müller, NTNU
Phil Schwarz, CSIRO
Akio Tomiyama, Kobe University
Hans Kuipers, Eindhoven University of Technology
Jinghai Li, Chinese Academy of Science
Markus Braun, Ansys
Simon Lo, CD-adapco
Patrick Segers, Universiteit Gent
Jiyuan Tu, RMIT
Jos Derksen, University of Aberdeen
Dmitry Eskin, Schlumberger-Doll Research
Pär Jönsson, KTH
Stefan Pirker, Johannes Kepler University
Josip Zoric, SINTEF

CONTENTS

EXPERIMENTAL AND NUMERICAL INVESTIGATION OF A BUBBLING DENSE GAS-SOLID FLUIDIZED BED

Lei YANG[1], J.T. PADDING [2*], J.A.M. KUIPERS[1]

[1] TUE Department of Chemical Engineering and Chemistry, 5600MB Eindhoven, the Netherlands

[2] TUD Department of Process and Energy, 2826BL Delft, the Netherlands

Corresponding author's e-mail: J.T.Padding@tudelft.nl

ABSTRACT

Eulerian models incorporating kinetic theory of granular flow (KTGF) are widely used to simulate gas-solids flow. The most widely used KTGF models have been derived for dilute flows of slightly inelastic, frictionless spheres. In reality, however, granular materials are mostly frictional. Attempts to quantify the friction effect have been somewhat limited. In this work, we focus on the validation of the KTGF model for rough spheres derived by Yang et al. (2016a, b) and the corresponding BCs from Yang et al. (2016c) for frictional walls. The present TFM simulations are validated by comparing with magnetic particle tracking (MPT) experimental data and results obtained from discrete particle model (DPM) simulations of a pseudo-2D bubbling fluidized bed. Numerical results are compared with respect to particle distribution, solids velocities, and energy balance in the bed. On comparison with a simple kinetic theory derived by Jenkins and Zhang (2002), we find that present model improves the predictions for particle axial velocity and flux upon simulation of inelastic rough particles. In conclusion, the current KTGF model obtains excellent agreement with experiment and discrete particle simulation for the time-averaged bed hydrodynamics.

NOMENCLATURE

e	normal restitution coefficient
p	pressure, Pa
$\mathbf{v}$	velocity, m/s
$\mathbf{F}$	force, N
m	mass, kg
$\mathbf{T}$	torque, Nm
ρ	density, kg/m^3
Θ	granular temperature, m^2/s^2
β_0	tangential restitution coefficient
σ	particle diameter, m
γ	energy dissipation rate, kg/(m·s^3)
β_A	inter-phase momentum transfer coefficient
$\boldsymbol{\tau}$	stress tensor, Pa
ε	volume fraction
$\boldsymbol{\omega}$	rotational velocity, rad/s
κ	thermal conductivity, kg/(m·s)
$\mathbf{g}$	gravitational acceleration, m/s^2

INTRODUCTION

Gas-solid fluidized beds are widely encountered in the chemical, petrochemical, metallurgical industries due to high heat and mass transfer rates resulting from large gas-solids contact. In order to improve existing processes and scale up new processes, the hydrodynamics of gas-solids fluidized beds need to be better understood. However, obtaining sufficient experimental data can be difficult, costly and becomes more complicated for large scale systems. Thus, with increasing computational power and more efficient numerical solver, numerical modelling becomes critical in complementing experimental investigation to provide valuable insights into gas-solids flow.

The continuum two fluid model (TFM) incorporated with kinetic theory of granular flow (KTGF) is commonly used for simulation of industrial scale gas-fluidized beds. In this approach, constitutive equations are solved using additional closure equations for particle phase (Kuipers et al., 1992). The most widely used KTGF models (Ding and Gidaspow, 1990; Nieuwland, 1996) have been derived for dilute flows of slightly inelastic, frictionless spheres. However, granular materials are mostly frictional in reality. Attempts to quantify the friction effect have been somewhat limited. Yang et al. (2016a) derived a kinetic theory of granular flow (KTGF) for frictional spheres in dense systems which includes the effects of particle rotation and friction explicitly. Moreover, this theory has been validated by Yang et al. (2016b) for the simulation of a dense solid-gas bubbling fluidized bed.

Both experiments by Sommerfeld and Huber (1999) and numerical simulations, e.g. Lan et al. (2012) and Loha et al. (2013), have reported the importance of wall boundary conditions in determining the characteristics of granular flow. However, there is no consensus on the value of this coefficient. Moreover, the physical meaning is not clear. In rapid granular flows, a rapid succession of almost instantaneous collisions between particles and wall cause random fluctuations of the particle velocities, which determine the amount of momentum and fluctuation energy transferred through the walls (Louge, 1994). Yang et al. (2016c) derived new boundary conditions (BCs) for collisional granular flows of spheres at flat frictional walls. They characterized the influence of frictional wall by the normal and tangential restitution coefficients and friction coefficient. Their theory described the collisions between frictional particles and flat walls physically, and adopted both rotational and translational granular temperature. They performed simulations of a bubbling pseudo-2D

fluidized bed using new BCs. The results showed that the new BCs were better capable of predicting solids axial velocity profiles, solids distribution near the walls. However, the most noticeable effect was the better agreement of rotational granular temperature with that from DPM simulations.

Even though numerical simulations are widely used to predict detailed understanding of flow structures in fluidized beds. However, validation of those numerical models using advanced and detailed experiments are still crucial. Due to the opaqueness of fluidized beds, non-invasive techniques are preferred like electrical resistance tomography, electrical capacitance tomography, positron emission particle tracking and magnetic resonance imaging. MPT has been emerged as a promising tool to investigate hydrodynamics in the process of fluidization due to its long-term stability and low computational effort. This method uses a magnetic tracer particle, which follows the bulk particle flow and is continuously detected by multiple magnetic field sensors located outside the bed. In MPT, a series of anisotropy magnetoresistive sensors detect the instantaneous position and orientation of the magnetic tracer. Based on statistical analysis of the tracer trajectory, characteristic measures of the bulk particle flow, such as the average particle velocity and particle circulation pattern, can be determined as a function of operating conditions. The application of magnetic particle tracking (MPT) in fluidization has been first initiated by Mohs et al. (2009) for the study of a spouted bed. Recently, MPT improved by Buist et al. (2015) has been employed in dense granular flow of bubbling fluidized beds.

The present study focuses on the validation of the present KTGF model and the corresponding BCs from Yang et al. (2016c) for rough walls. Experimental work of Lorenz et al. (1997) reported several impact properties for collisions of small, nearly spherical particles. Due to limited choice of magnetic tracker, we adopted the stainless steel 316 which is non-magnetisable and has a quite rough surface. A systematic quantitative comparison among Eulerian-Eulerian two fluid simulation, DPM and one-to-one MPT experiment is carried out in a pseudo 2D bubbling fluidized bed. In particular, we investigate the effect of different inlet gas velocities on the hydrodynamics in the bed. We compare the time- and space- averaged quantities, i.e. particle velocity, particle flux, particle circulation pattern and distribution. The aim of this comparison is to show the level of agreement between simulations and experiments encountered in particle phase. Further, a careful comparison is made between the present model and the effective model by Jenkins and Zhang (2002) (represented as old TFM).

NUMERICAL MODELS

Two fluid model

The two fluid model describes both gas phase and solid phase as fully interpenetrating continua. The continuity equations for gas and solid phases are given in equation 2.1 with the subscript k denoting the gas ($k = g$) or solid ($k = s$). The momentum equations are given by 2.2 and 2.3.

$$\frac{\partial(\varepsilon_k \rho_k)}{\partial t} + \nabla \cdot (\varepsilon_k \rho_k \mathbf{v}_k) = 0 \tag{1}$$

$$\frac{\partial(\varepsilon_g \rho_g \mathbf{v}_g)}{\partial t} + \nabla \cdot (\varepsilon_g \rho_g \mathbf{v}_g \mathbf{v}_g) = -\nabla \cdot (P_g \mathbf{I} + \varepsilon_g \boldsymbol{\tau}_g) + \varepsilon_g \rho_g \mathbf{g} - \beta_A (\mathbf{v}_g - \mathbf{v}_s) \tag{2}$$

$$\frac{\partial(\varepsilon_s \rho_s \mathbf{v}_s)}{\partial t} + \nabla \cdot (\varepsilon_s \rho_s \mathbf{v}_s \mathbf{v}_s) = \varepsilon_s \rho_s \mathbf{g} - \nabla \cdot (P_s \mathbf{I} + \varepsilon_s \boldsymbol{\tau}_s) + \beta_A (\mathbf{v}_g - \mathbf{v}_s) - \varepsilon_s \nabla P_g \tag{3}$$

The gas and solid phases are coupled through the interphase momentum transfer coefficient β_A. To describe the solid phase, KTGF with friction is used. In this work, particle surface friction and rotation are considered explicitly. In order to describe the solid phase rheology thoroughly, an extra energy balance equation for the rotational granular temperature was derived.

$$\frac{3}{2}\left[\frac{\partial(\varepsilon_s \rho_s \Theta_t)}{\partial t} + \nabla \cdot (\varepsilon_s \rho_s \mathbf{v}_s \Theta_t)\right] = -3\beta_A \Theta_t - \nabla \mathbf{v}_s : (P_s \mathbf{I} + \varepsilon_s \boldsymbol{\tau}_s) + \varepsilon_s \nabla \cdot (\kappa_t \nabla \Theta_t) - \gamma_t \tag{4}$$

$$\frac{3}{2}\left[\frac{\partial(\varepsilon_s \rho_s \Theta_r)}{\partial t} + \nabla \cdot (\varepsilon_s \rho_s \mathbf{v}_s \Theta_r)\right] = \varepsilon_s \nabla \cdot (\kappa_r \nabla \Theta_r) - \gamma_r \tag{5}$$

The definitions of the translational and rotational granular temperatures are respectively $\Theta_t \equiv \left\langle C^2 \right\rangle / 3$, $\Theta_r \equiv I \left\langle \Omega^2 \right\rangle / 3m$, where I is particle's moment of inertia, C is the fluctuating translational velocity and Ω is the fluctuating angular velocity. All the closures can be referred to Yang et al. (2016a).

Additionally, it is know that BCs on the gas and solid phases velocities and solid granular temperature, need to be specified at the wall. In the simulations, a no-slip wall boundary condition for side walls (left, right, front and back side of the rectangular domain) is used for the gas phase. At the bottom inlet, a uniform gas velocity is specified, whereas at the top outlet, atmospheric pressure (101 325 Pa) is prescribed. For the solid phase, a partial slip boundary condition is used for the side walls. We applied the relations for solids velocity gradient, translational and rotational energy dissipation rate per unit area derived by Yang et al. (2016c). The boundary conditions for solid velocity and granular temperatures at a flat frictional wall have the form

$$-\left(\mu_{t_s} + \mu_{r_s}\right)\frac{\partial v_i}{\partial n} = \mu mn(1+e) g_0 \cot\theta_c \frac{\Theta_t V_i}{\sqrt{2\pi\Theta_t}} \max(A1, A2) \tag{5}$$

$$-\kappa_t \frac{\partial \Theta_t}{\partial n} = Q_t \tag{7}$$

$$-\kappa_r \frac{\partial \Theta_r}{\partial n} = Q_r \tag{8}$$

where n is direction perpendicular to the wall and i is the velocity component. V_i is the local mean contact velocity. μ_{t_s} and μ_{r_s} are the shear viscosities based on the KTGF of Yang et al. (2016a). A1 and A2 are functions regarding three measurable collisional parameters, rotational and translational granular temperatures and slip velocity. The details expressions can be referred to the Appendix and Yang et al (2016c).

Discrete particle model

In DPM, the gas phase is described in the same way as in TFM (equations 2.1 and 2.2). However the solid phase is treated more detailed. The motion of every particle in the DPM is computed with Newton's second law of motion,

$$m_p \frac{d\mathbf{v}_p}{dt} = \sum \mathbf{F} = \mathbf{F}_{external} + \mathbf{F}_{contact}$$
$$I \frac{d\boldsymbol{\omega}}{dt} = \mathbf{T} \qquad (9\text{-}10)$$

where m_p, $\mathbf{v}_p$, $\mathbf{T}$ are particle mass, velocity, and torque acting on the particle. The sum of all external forces acting on a particle $\mathbf{F}_{external}$ is calculated using:

$$\mathbf{F}_{external} = m_p \mathbf{g} - V_p \nabla p_g + \frac{V_p \beta_A}{1-\varepsilon_g}\left(\mathbf{v}_g - \mathbf{v}_p\right) \qquad (11)$$

where V_p is the volume of particle. We use a linear spring-dashpot contact force, where the friction coefficient μ is limiting the tangential contact force:

$$\mathbf{F}_{contact,n} = -k_n \delta_n \mathbf{n}_{ab} - \eta_n \mathbf{v}_{ab}$$
$$\mathbf{F}_{contact,\mathrm{t}} = \begin{cases} -k_t \delta_t - \eta_t \mathbf{v}_{ab,t}, & \text{(sticking)} \\ -\mu \left|\mathbf{F}_{contact,n}\right| \mathbf{t}_{ab}, & \text{(sliding)} \end{cases} \qquad (12\text{-}13)$$

where k_n, $\mathbf{n}_{ab}$, δ_n, η_n, $\mathbf{v}_{ab}$, δ_t, η_t are respectively the spring stiffness in the normal direction, the normal unit vector, the overlap and damping coefficient in the normal direction, relative velocity at the contact point, and the overlap and damping coefficient in the tangential direction. We do not include a rolling friction. We refer to Hoomans et al. (1996) for details on the DPM model.

Parameters	Values
Particle type	Stainless steel 316
Particle density, kg/m^3	8000
Particle diameter (mm),	3.0
Initial bed height (m),	0.15
Domain size (m),	0.15 × 0.015 × 1.0
Grid number (x × y ×z)	15 × 2 × 60
p-p collisional parameters,	e_n=0.91, β_0=0.33, μ=0.15
p-w collisional parameters,	e_w=0.93, β_w=0.40, μ_w=0.13
Superficial gas velocity,	3.75 m/s
Simulation time	35 s
Flow solver time-step	10^{-4} s

Table 1: Properties of particles and simulation settings.

MODEL VALIDATION

Simulation settings

In the old TFM, we employ the same BCs for the gas phase. However, partial slip BCs from Sinclair and Jackson (1987) are used for four side walls with a specularity coefficient of 0.2. The simulation settings are specified in Table 1. In the experiment, the pseudo 2D bed has the same height, width and depth as is in the simulation. The four side walls are made of plastic glass. The porous distributor plate made of bronze has an average pore size of 10 μm and a thickness of 3 mm. The distance between the measuring domain and the sensors is maintained less than 2 cm during experiment. To ensure statistical data, experiments are carried out for 2.5-3.0 h. The averaged bed dynamics are inferred from the motion of the tracker. The principle of the MPT measurement technique has been given by Buist et al. (2015). We followed the same method to filter data and deal with the corresponding post-process. Finally, an overview of all settings and properties is listed in Table 1.

Results and discussion

In the experiment, we found that the minimum fluidization velocity is 3.91 m/s. Meanwhile the minimum fluidization velocity is 3.75 m/s in the simulation with the Ergun/Wen and Yu drag law. In the present pseudo 2D bed, the depth is only 5 times larger than the particle diameter, which reveals that particle bridge can occur. Consequently, this bridging leads to difficulties in determining local drag. This explains the mismatch of the minimum fluidization velocity between the experiment and the simulation. To make comparison with MPT experiment, we adopted the same excess background velocity. In this part, we focus on the validation of our current KTGF model and BCs for rough spheres impacting on a flat frictional wall.

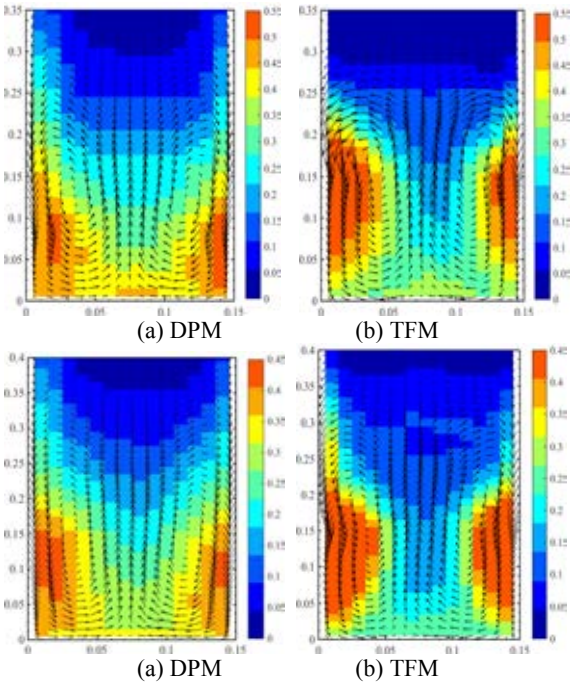

(a) DPM (b) TFM

(a) DPM (b) TFM

Figure 1: Time-averaged (10-35s) solids flux pattern and solids volume distribution at various superficial gas velocity, top row: Ug = 1.5Umf; bottom row: Ug = 2.0 Umf.

In order to study the overall behaviour of the bubbling bed, the time-averaged volume distribution and solids flux pattern are plotted in **Figure 1**. The DPM simulations show dense zones of solids close to the side walls and at the bottom of the bed. This type of solids volume fraction distribution reveals that bubbles are mostly formed at the bottom and move towards the center. On the other hand,

animations of the porosity patterns indicate that in TFM simulations more bubbles than in DPM are generated at the bottom of the bed and larger bubbles are formed (due to coalescence) in the center of the bed. Therefore, the DPM simulations, produces slightly more dilute zones in the lower part of the bed and more dilute zones in the center, and consequently larger dense zones near the side walls in comparison with the TFM simulations. Besides, the very low solids concentration at the top of the bed from both DPM and TFM simulations indicates the bursting of bubbles. With increasing superficial gas velocity, in both DPM and TFM simulations bubble coalescence is enhanced and more pronounced lateral motion of bubbles occurs, leading to a more dilute zone in the center of the bed.

TFM and DPM simulations show very similar solids flux pattern. Particles move laterally close to the distributor, flow upwards in regions of more intense bubble activity and downwards in regions of lesser bubble activity. Consequently, a pronounced global solids circulation pattern with two symmetric vortices in the middle of the bed is formed. Since the height of the dense zone grows due to the increasing superficial gas velocity. It can be noticed that the size of the vortices has enlarged, which was also observed by Lindborg et al. (2007).

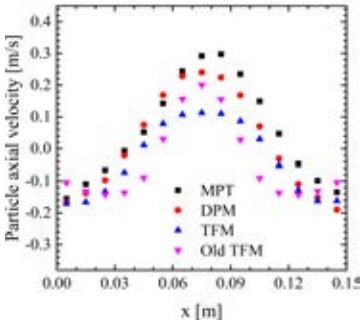

(a) height=0.05 m

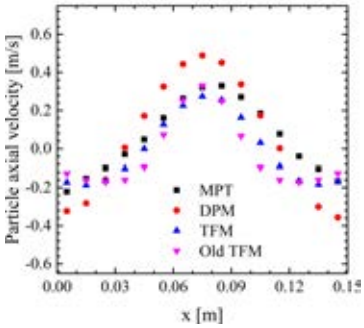

(b) height=0.1 m

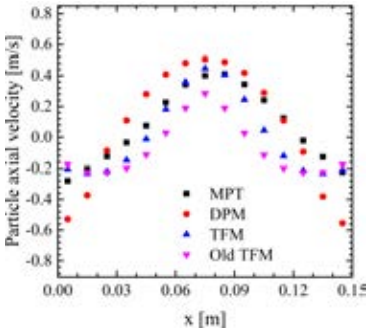

(c) height=0.15 m

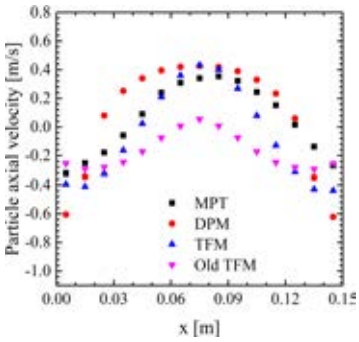

(d) height=0.2 m

Figure 2: Comparison of the time-averaged (10-35s) particle axial velocity between MPT experiment, DPM and TFM simulations at various heights, Ug = 1.5Umf.

Figure 2 overlays the profiles of time-averaged particle axial velocity at different heights measured in the experiment and the numerical simulations at Ug = 1.5Umf. Overall, the particles ascend in the center and descend near the side walls due to the preferred path of the rising bubbles. Note that rough wall BCs are employed also at the bottom wall in our TFM simulations, which probably hinders particle upwards motion close to the distributor. Additionally, in the dense bottom region, long-term and multi-particle collisions are dominant, which are not accounted for in the TFM simulations. As a consequence, the new TFM simulations underpredict the particle velocity in the center at the lower height of 0.05 m (**Figure 6.2(a)**),but produce good agreement near the wall and in the annulus. At all other heights, a good match is obtained among the new TFM, DPM simulations and MPT experiments in the bulk. In contrast, the old TFM obtains good agreement with the MPT experiments and DPM simulations in the lower part of the bed, but underpredicts the particle axial velocity in the upper parts of the bed. In the dense wall region, DPM overestimates the downward solid velocity. This deviation between MPT experiments and DPM simulation was also reported by Buist et al. (2015) for a bubbling bed. They pointed out that it was necessary to add particle rolling friction to make corrections. However, the present TFM simulations are in excellent agreement with the experiments.

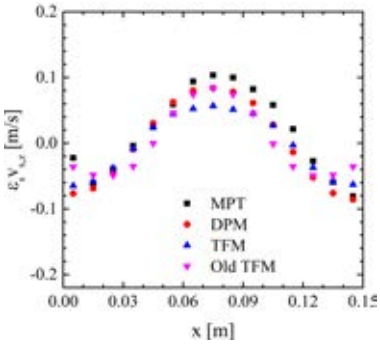

(a) height=0.05 m

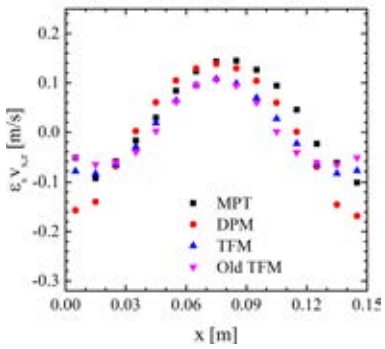

(b) height=0.1 m

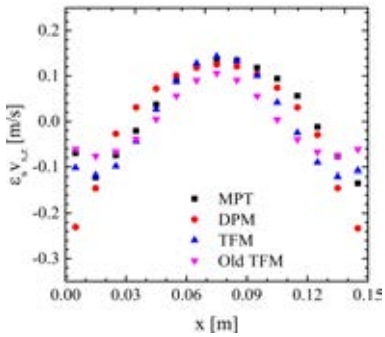

(c) height=0.15 m

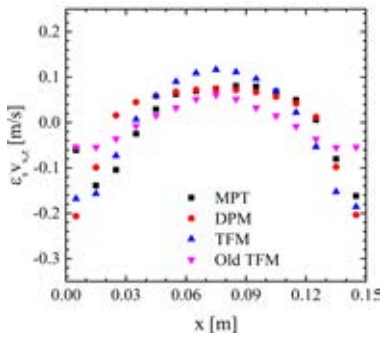

(d) height=0.2 m

Figure 3: Comparison of the time-averaged (10-35s) particle axial flux between MPT experiment, DPM and TFM simulations at various heights, Ug = 1.5Umf.

Figure 3 shows the downward and upward particle axial flux for different heights from experiment and simulations at a background velocity of Ug = 1.5 Umf. The upward solid flux is located in the center and the downward solid flux is observed in the near wall region. As can be seen from **Figure 1(a)** and **2(a)**, the upward solid flux close to the distributor is underestimated in present TFM simulations as a consequence of rough wall BCs at the bottom. Small bubbles are generated close to the distributor and side walls, carry particles in their wakes, which produces voids filled by downward owing particles. Due to the coalescence of these bubbles, the amount of downward solids flux increases with increasing bed height, particularly in the near wall region. As bubbles move up in the bed center, particles ow vertically upward at higher axial area (0.05-0.15 m), which indicates an increase in upward solids flux. The number of particles close to the freeboard is so limited that lower amount of upwards solids flux is observed at the height of 0.2 m. All of these corresponds well to the results in **Figure 1**. In total, current TFM, old TFM and DPM simulations are in good agreement with the experiment.

Figure 4 shows profiles of the particle axial velocities at various heights from experiment and simulations at Ug = 2.0 Umf. In general, the current TFM simulations agree well with the results from DPM and the experiment. Due to the roughness of the distributor, both TFM simulations under estimate the particle axial velocity. Unfortunately, the old TFM from Jenkins and Zhang (2002) under predicts particle axial velocity in the center and captures lower amount of particle velocity value close to the wall. Similar underestimation of particle axial velocity is reported in the work of Lu and Gidaspow (2003). The particle surface friction leads to the formation of bed heterogeneous structures. For rough particles, more energy is dissipated during particle-particle and particle-wall collisions.

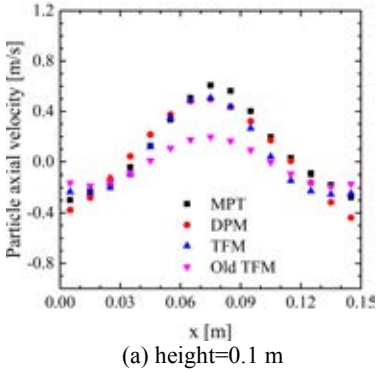

(a) height=0.1 m

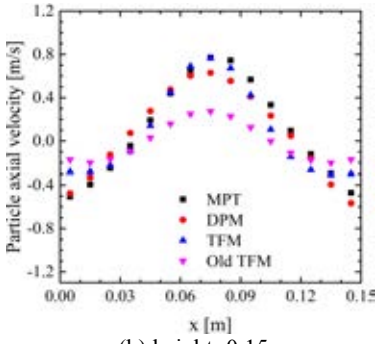

(b) height=0.15 m

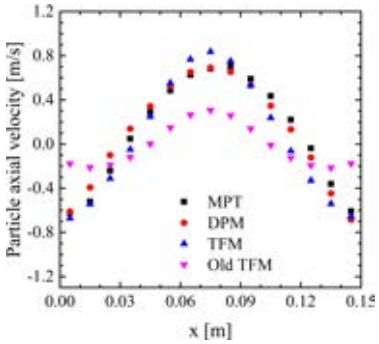

(c) height=0.2 m

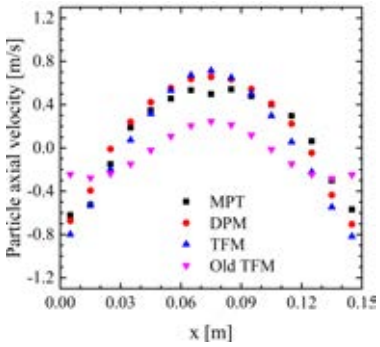

(d) height=0.25 m

Figure 4: Comparison of the time-averaged (10-35s) particle axial velocity between MPT experiment, DPM and TFM simulations at various heights, Ug = 2. Umf.

Comparisons of the time-averaged solid flux are depicted in **Figure 5**. In all cases, the current TFM simulations obtain best match with the DPM simulations among the results from MPT experiment and the old TFM. Note that characteristic measurements of the bulk particle ow is based on statistical analysis of the tracer trajectory in MPT experiment. Consequently, the MPT experiment just provides the information of $<\varepsilon_s><v_s>$. In contrast, $<\varepsilon_s v_s>$ is applied in simulations. It is clear that $<\varepsilon_s v_s>$ is not equal to $<\varepsilon_s><v_s>$. Thus, for this part we focus on the comparisons among simulations. With increasing height, both TFM simulations are in better accordance with the DPM simulation. Finally, the current TFM achieves significant improvement of the modelling results.

Time-averaged bubble size and count are presented in **Figure 6** to investigate the bubble motion. Note that the equivalent bubble diameter is evaluated using the bubble area A, i.e. De = $\sqrt{4A/\pi}$ particle value of gas fraction equal to 0.8 is applied as the bubble boundary. Moreover, we exclude bubbles in contact with the free-board to avoid ambiguity. **Figure 6(a)** shows that the bubble size increases with increasing bed height. As is shown in **Figure 6(b)**, large number of bubbles near the bottom indicates that small bubbles emerge, and less bubbles with increasing bed height reveals the bubble coalescence. The old TFM predicts larger bubble size and less bubbles than the DPM and present TFM models. This is due to the fact that bubbles from the DPM and present TFM simulations burst into the free-board and form an obvious slugging fluidization.

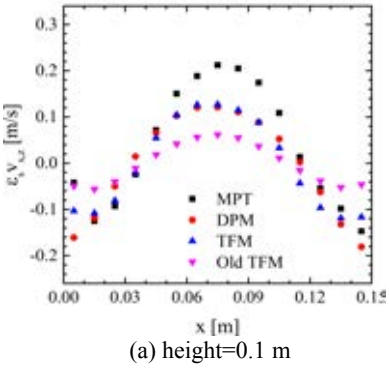

(a) height=0.1 m

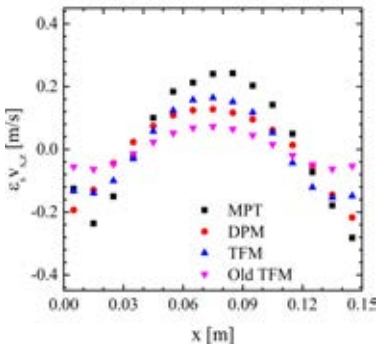

(b) height=0.15 m

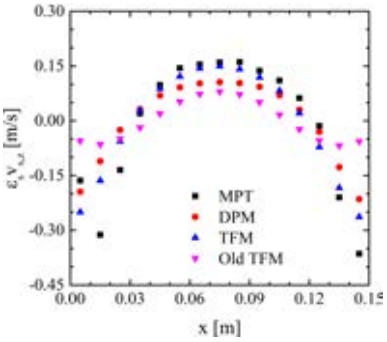

(c) height=0.2 m

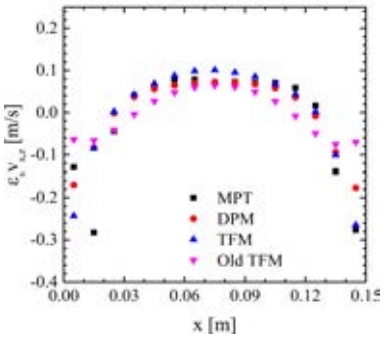

(d) height=0.25 m

Figure 5: Comparison of the time-averaged (10-35s) particle axial flux between MPT experiment, DPM and TFM simulations at various heights, Ug = 2.0Umf.

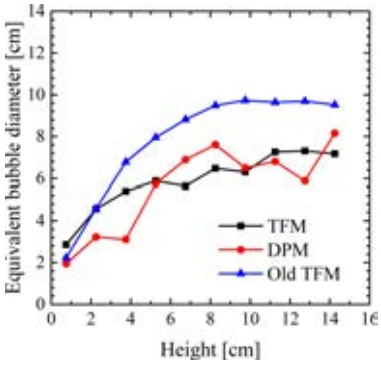

(a)

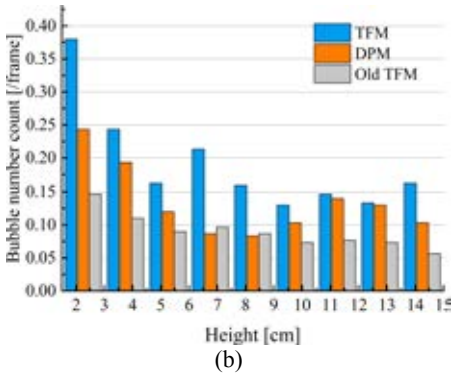

(b)

Figure 6: Comparison of time-averaged (10-25s) equivalent bubble diameter at different height, Ug = 1.5Umf.

CONCLUSION & OUTLOOK

This work focus on the validation of the present KTGF model for rough spheres and the corresponding BCs for rough wall. Current KTGF model are validated by comparing with one-to-one MPT experiment and DPM simulations of the same dense solid-gas fluidized bed both in a pesudo-2D. We have performed comparisons between the present KTGF model and the results of a simple kinetic theory derived by Jenkins and Zhang (2002). On comparison with DPM simulation and MPT experiment, it can be concluded that our present model improves the predictions obtained from the Jenkins and Zhang's model for the simulation of inelastic rough particles. The energy distributions from the current TFM is almost the same as that from DPM simulation. Consequently, Jenkins and Zhang's model under predicts particle axial velocity in the bed center and captures lower amount of particle velocity close to the wall, especially at high superficial fluidization velocity. Then, because of including of particle surface friction and rotation, larger densely packed zones are formed both in DPM and present TFM simulations, which is not clear in the old TFM simulation. In conclusion, further validation of current TFM for type Geldart A and B should be carried out. Additionally, since industrial fluidized beds are generally large and cylindrical in shape, therefore validation of current TFM model in cylindrical bed is also necessary.

REFERENCES

HOOMANS, B.P.B., et al., (1996), "Discrete particle simulation of bubble and slug formation in a two-dimensional gas-fluidised bed: a hard-sphere approach". *Chemical Engineering Science* **51(1)**, 99-118.

JENKINS, J.T. and ZHANG, C., (2002), "Kinetic theory for identical, frictional, nearly elastic spheres". *Physics of Fluids*, **14**, 1228-1235.

LOUGE, M.Y. (1994), "Computer-simulations of rapid granular flows of spheres interacting with a flat, frictional boundary". *Physics of Fluids* **6**, 2253-2269.

LAN, X., et al., (2012), "Influence of solid-phase wall boundary condition on CFD simulation of spouted beds". *Chemical Engineering Science* **69(1)**, 419-430.

LOHA, C. et al., (2013), "Euler-Euler CFD modelling of fluidized bed: Influence of specularity coefficient on hydrodynamic behaviour". Particuology **11** 673-680.

KUIPERS, J. A. M., et al., (1992), "A numerical model of gas-fluidized beds". *Chemical Engineering Science* **47**, 1913-1924.

DING, J. M., and GIDASPOW, D., (1990), "A bubbling fluidization model using kinetic theory of granular flow". *AIChE Journal* **36**, 523-538.

NIEUWLAND, J. J., et al., (1996), "Hydrodynamic modelling of gas/particle flows in riser reactors". *AIChE Journal* **42(6)**, 1569-1582.

SOMMERFELD, M. and HUBER N. (1999), "Experimental analysis and modelling of particle-wall collisions". *Int. J. Multiphase Flow* **25**, 1457-1489.

LINDBORG, H., et al., (2007), "Practical validation of the two-fluid model applied to dense gas–solid flows in fluidized beds". *Chemical Engineering Science* **62(21)**, 5854-5869.

LORENZ, et al., (1997). "Measurements of impact properties of small, nearly spherical particles". *Experimental Mechanics* **37(3)**, 292-298.

SINCLAIR, J., JACKSON R., (1987), "Gas-Particle Flow in a Vertical Pipe with Particle-Particle Interactions". *AIChE Journal* **35** 1473-1486.

Yang, L., et al., (2016a), "Modification of Kinetic Theory for Frictional Spheres, Part I: Two-fluid model derivation and numerical implementation". *Chemical Engineering Science* **152**, 767-782.

Yang, L., et al., (2016b), "Modification of kinetic theory of granular flow for frictional spheres, part II: Model validation". *Chemical Engineering Science* **152**, 783-794.

Yang, L., et al., (2016c), "Partial slip boundary conditions for collisional granular flows at flat frictional walls". *AIChE Journal*, 10.1002/aic.15534

LU, H.L., GIDASPOW, D., (2003). "Hydrodynamics of binary fluidization in a riser: CFD simulation using two granular temperatures". *Chemical Engineering Science* **58(16)**, 3777-3792.

MOHS, G., et al., (2009). "Magnetic monitoring of a single particle in a prismatic spouted bed". *Chemical engineering science* **64(23)**, 4811-4825.

BUIST, K. A., et al., (2015). "Determination and comparison of rotational velocity in a pseudo 2D fluidized bed using magnetic particle tracking and discrete particle modelling". *AIChE Journal* **61(10)**, 3198-3207.

ACKNOWLEDGEMENT

The authors thank the European Research Council for its financial support, under its Advanced Investigator Grant scheme, Contract no. 247298 (Multi-scale Flows).

APPENDIX

The expressions in the BCs for particle slip velocity are as follows,

$$A1 = \frac{1}{2\left(1+X^2\right)} + \frac{Y^2\left(1-X^2\right)}{8X^2\left(1+X^2\right)^2} + \frac{\left(4X^2-Y^2\right)\arctan\left[X\right]}{8X^3}$$

$$A2 = \frac{\sqrt{\pi}}{2Y}\operatorname{erf}\left(Y\right) - \frac{X^2 e^{-Y^2}\left(2Y^2-1\right)}{4Y^2} - \frac{\sqrt{\pi}X^2}{8Y^3}\operatorname{erf}\left(Y\right)$$

Where $X = \sqrt{1+\lambda}\cot\theta_c$, $Y = \sqrt{\frac{V_t^2}{2\Theta_t}}\cot\theta_c$

The corresponding boundary conditions for granular temperatures are

$$-\kappa_t \frac{\partial \Theta_t}{\partial n} = g_0 \rho_s \varepsilon_s \left\{ \mu^2 \left(1+e\right)^2 \left(1 - \frac{e^{-\frac{Y^2}{1+X^2}}}{1+X^2} \right) - (1-e^2) \right\} \sqrt{\frac{\Theta_t}{2\pi}} \Theta_t$$

$$+ g_0 \rho_s \varepsilon_s \frac{2\left(1+\beta\right)}{7} (1+\lambda) \frac{2-ee_p}{2+ee_p} \min \left[\begin{matrix} \left(2\Theta_t (1+\lambda) B1 - V_t^2 A1\right), \\ V_t^2 \left(B2 - A2\right) \end{matrix} \right] \sqrt{\frac{\Theta_t}{2\pi}}$$

$$-\kappa_r \frac{\partial \Theta_t}{\partial n} = \frac{5}{4} (1+e)^2 \mu^2 m n g_0 \Theta_t \frac{2-ee_p}{2+ee_p} \sqrt{\frac{2\Theta_t}{\pi}} \left(1 - \frac{e^{-\frac{Y^2}{1+X^2}}}{1+X^2} \right)$$

Where

$$B2 = \frac{\sqrt{\pi}}{2Y} \operatorname{erf}\left(Y\right) + \frac{X^2\sqrt{\pi}}{8Y^3} \operatorname{erf}\left(Y\right) + \frac{3-2Y^2}{4Y^2} X^2 \mathrm{e}^{-Y^2} + \frac{\sqrt{\pi} X^4}{64Y^5} \operatorname{erf}\left(Y\right)$$

$$B1 = \frac{2X^2(X^2+1) + Y^2(X^2 - Y^2 + 3)}{4X^2\left(1+X^2\right)^2} + \frac{3Y^4\left(1+7X^4\right)}{96X^4\left(1+X^2\right)^3}$$

$$+ \frac{8X^2\left(2X^2+Y^2\right) - Y^4}{32X^5} \arctan X$$